Computational Analysis of Subcooled Flow Boiling in a Vertical Minichannel with Two Different Shapes under Various Mass Fluxes

A. Igaadi [†], H. El Mghari and R. El Amraoui

Laboratory of Energy and Materials Engineering (LEME), Faculty of Sciences and Technologies (FST), Sultan Moulay Slimane University (SMSU), Beni Mellal, Morocco

†*Corresponding Author Email: amal.igaadi@usms.ma*

ABSTRACT

In the current research project, two-dimensional numerical simulations are conducted to analyze the effects of geometrical configuration on flow structures and the thermal performances of subcooled flow boiling. The CFD simulations are carried out in two different configurations (straight and periodic constriction expansion) in a minichannel mounted vertically at four mass fluxes (500 kg/m²s; 836.64 kg/m²s; 1170 kg/m²s; and 2535 kg/m²s). The present predicted results exhibit excellent accordance with the previous experiments, with mean errors of 6.39% and 9.78%, demonstrating the efficiency of the present numerical study. The simulation results show that the periodic constriction expansion design provides good mixing between the layers, leading to a 43.11% mean enhancement of the thermal transfer, which is more important than the slight pressure drop penalty of 4.32 for a mass flux of 500 kg/m²s due to the combined pressure drop along the minichannel that resulted from the periodic constriction and expansion regions. Furthermore, the visualization of flow patterns shows that the bubbly flow is the dominant flow regime in the periodic constriction-expansion configuration.

1. INTRODUCTION

The latest miniaturization of devices in a wide variety of industries such as semiconductor lasers, electronics, aerospace, medicine, and biotechnology (McGlen et al., 2004; Zhou et al., 2016; Ramasamy et al., 2018) has led to a fast increase in heat generation, which leads to a critical thermal management issue. Therefore, this necessitates the implementation of a small-scale cooling system that balances energy efficiency and sustainability.

The miniature thermal technologies based on the subcooled flow boiling process allow for the absorption of high heat flux and maintain a uniform temperature distribution with a low inventory of the working fluid compared to the single-phase methods (Agostini et al., 2007; Kandlikar, 2012). The above factors provided this particular cooling technology type with excellent heat removal ability and made it one of the most successful approaches to meeting the challenges of cooling the high heat fluxes encountered in various fields. However, the complicated phase change process at the interface makes subcooled flow boiling often subject to much flow instability, which is not completely understood yet, especially for small-scale systems where the interface

itself is difficult to determine (Boure et al., 1973; Kennedy et al., 2000; Tardist, 2007). As a result, studying subcooled flow boiling along minichannels is critical for fully understanding this process, improving heat transfer performance, and guiding their design for safe operation. The majority of subcooled flow boiling research has focused on bubble dynamics behavior (Ahmadi et al., 2012; Sugrue et al., 2014; Bahreini et al., 2015; Chen et al., 2020; Rena et al., 2020; Parahovnik et al. 2022), with relatively few studies of two-phase flow regimes as well as thermal transfer characteristics.

In general, several factors can affect the thermal performances of subcooled flow boiling, such as mass flux (Sugrue et al., 2014; Bahreini et al., 2015), imposed heat flux (Sugrue et al., 2014; Hożejowska et al., 2016), pressure (Sugrue et al. 2014; Markal et al., 2018a,b; Parahovnik & Peles, 2022), physical properties of the working fluid (Ali & Palm, 2011; Liu et al., 2012; Liu & Bi, 2015; Vasileiadou et al., 2017; Azzolin & Bortolin, 2021; Chen et al., 2021), orientation (Sugrue et al., 2014; Gao et al., 2017; Igaadi et al., 2023) and gravity levels (Bower & Klausner, 2006; Brutin et al., 2013; Bahreini et al., 2016; Lebon et al., 2019; Iceri et al., 2020).

Nomenclature				
E	energy	**Greek symbols**		
F_{csf}	surface tension force	α	volume fraction	
g	gravity acceleration	λ	conductivity	
G	mass flux	ρ	density	
h	heat transfer coefficient	μ	dynamic viscosity	
h_{lv}	specific latent heat	σ	surface tension coefficient	
q	heat flux	ξ	local interface curvature	
u	flow velocity	**Subscript**		
u_t	friction velocity	*eff*	effective	
P	pressure	*in*	inlet	
S	source term	*l*	liquid phase	
t	time	*lv*	liquid vapor mixture	
Δt	time step	*sat*	saturation temperature	
T	temperature	*v*	vapor phase	
		w	wall	

The wettability of heated surfaces can also affect the process of subcooled flow boiling, as demonstrated by Ahmadi & Okawa (2015), who reported that for a hydrophilic heated surface, all bubbles exited the nucleation sites immediately after nucleation, and the opposite for a hydrophobic case.

Whereas, Phan et al. (2011) tested a variety of hydrophilic and hydrophobic surfaces with different static contact angles (26, 49, 63, and 103). They demonstrated that as the static contact angle increases, so does the pressure drop.

Apart from studying the influence of different thermal and physical parameters, it is also necessary to search for techniques that can be used to further improve the performance of subcooled flow boiling process. Generally, several techniques could be used to improve the thermal transfer performances of this process, including the use of enhanced surfaces, which are distinguished by their high heat transfer enhancement due to the large number of nucleation sites that they can provide, as demonstrated in several previous studies (Sun et al., 2011; Piasecka, 2012, 2013, 2014; Şişman et al., 2016; Nedaei et al, 2017; Piasecka & Strąk 2019; Hsu et al., 2022). Furthermore, the addition of nano-scale particles to the working fluids represents another option for improving heat transfer in the subcooled flow. Kim et al. (2010) added alumina, zinc oxide, and diamond nanoparticles to the water. They found that the critical heat flux is improved by up to 50% more than that of water as a base fluid. While studying the graphene oxide (GO)/water nanofluid, Lee et al. (2013) discovered that the critical boiling heat flux (CHF) of the GO/water nanofluid was increased by 100% when compared to the CHF of water. Furthermore, in Al_2O_3/H_2O nanofluids examined by Wang and Wu. (2015), it was indicated that the bubble grows faster and the bubble departure frequency is higher than that of water as a base working fluid. But the increase in nanoparticle diameter causes a decrease in bubble departure diameter (Huang et al., 2020; Huang & Pan, 2021).

Geometrical parameters of minichannels are another factor that affects the thermal-hydraulic performance of subcooled flow boiling. Prajapati et al. (2015) compared the boiling characteristics of three different channel configurations: uniform, divergent, and segmented finned. Their results showed that the bubble blockage problem was completely solved in the segmented design and partially solved in the divergent configuration. Also, the segmented finned design provided the highest heat transfer coefficient compared to the other two shapes. Similarly, Tiwari & Moharana (2021) compared the straight and wavy configurations. Their study concluded that the straight design results in flow blockage and drying due to the confined bubbles formed, which results in flow blockage and drying, but the wavy design enables the formation of only the smaller bubbles. The corrugated minichannel was studied by Chang et al. (2011), who found that the internal peaks of corrugated walls enhanced bubble nucleation. However, increased pressure drops and the formation of large bubbles in a relatively short time have led to a degradation of heat transfer performance in this configuration. Li et al. (2017) investigated a microchannel with and without triangular cavities. Their results showed that the configuration of triangular cavities expanded the heat transfer area, thus significantly improving the heat transfer coefficient (an increase of 9.88 and 1.55 times, for G = 83 and 442 kg/m²s, respectively), coupled with a small pressure drop (a reduction of 50.3% and 12.8%, for G = 83 and 442 kg/m²s, respectively), as compared to the simple rectangular microchannel. In a further work by Li et al. (2019), they have added rectangular fins to the triangular cavities. This new microchannel design exhibited a remarkably higher heat transfer coefficient than the simple microchannel, with a maximum increase of 300% and 51.6% for G = 83 kg/m²s and G = 442 kg/m²s, respectively. However, the pressure drop increased as a result of this addition of this rectangular fins. In addition, the study of Chai et al. (2013) about microchannels with periodic expansion-constriction cross sections showed an improvement of 1.8 times in the average Nusselt number for this new channel structure compared to the simple microchannel, however, the pressure drop of the microchannel with periodic expansion-constriction cross sections increases rapidly and is obviously higher when *Re* is between 300 and 750. Therefore, the optimization of the small cooling system efficiency by a modification of the minichannel geometrical structure is a compromise between heat

transfer improvement and pressure drop reduction. Thus, further research is required to find an optimal geometric structure, which increases heat transfer, as well as minimizes pressure drops. Our present study suggests a novel shape for the periodic expansion-constriction minichannel with a shape factor, and examined their impact on heat transfer and pressure drop.

As several studies (Manda et al., 2020, 2021, 2022) have shown that numerical analysis can be used to predict heat transfer characteristics and flow patterns of different flow regimes inside microchannels. This paper primarily develops a numerical analysis of subcooled flow boiling in a suggested configuration (periodic expansion-constriction) and compares its thermal properties to the straight design. The simulations are carried out by varying the mass flux (500, 836.64, 1170, and 2535 kg/m²s) at a constant heat flux and inlet temperature. The extremely important motivation of this paper is related to the best flow mixing provided by the periodic expansion and contraction sections.

2. MATHEMATICAL MODEL

A 2D numerical simulation of subcooled flow boiling in two different minichannel designs is performed in the current work. To reduce the complexity of the current model, we have assumed some simplifications that are outlined in our previous numerical study (Igaadi et al., 2023).

Generally, numerical simulation of unsteady liquid-vapor flows is complicated because of the unstable interface position between phases and the change of thermo-physical properties at the interface, which requires an intensive calculation effort.

The volume of fluid (VOF) model proposed by Hirt & Nichols (1981) offers a resolution to these challenges based on first identifying the movement of all phases and then modeling the evolution of location and the shape of the interface as a result. This model depends on the fact that each cell of the domain is filled with one or more immiscible phases. This means that each phase is denoted by its volume fraction (α_v and α_l). Therefore, the following different cases are possible:

1. The liquid phase occupies the cell if $\alpha_l = 1$;

2. The vapor phase occupies the cell if $\alpha_l = 0$;

3. Both phases are present in the cell if $0 < \alpha_l < 1$, therefore the availability of the interface in the cell.

It is important to mention that in each cell of the computational domain, the combined volume fractions of all phases must equal one, as in the following equation:

$$\alpha_l + \alpha_v = 1 \tag{1}$$

2.1 Governing Equations

Liquid-vapor interface tracking, in the volume-of-fluid model is accomplished by solving the continuity equation for the volume fraction of both the liquid and the vapor phases in the following way:

$$\frac{\partial}{\partial t}(\alpha_l \rho_l) + \nabla.(\alpha_l \rho_l \vec{u}) = S_l \tag{2}$$

$$\frac{\partial}{\partial t}(\alpha_v \rho_v) + \nabla.(\alpha_v \rho_v \vec{u}) = S_v \tag{3}$$

The details of mass source transfer rates (S_l and S_v) are presented in the subsection of phase change model (subsection 2.2).

Both phases in the VOF model share the same set of momentum and energy equations. Therefore, these equations are solved in the computational domain without making any distinction between phases. Consequently, they expressed themselves as follows:

Momentum equation:

$$\frac{\partial}{\partial t}(\rho \vec{u}) + \nabla.(\rho \vec{u}\vec{u}) = -\nabla P + \nabla.[\mu(\nabla \vec{u} + (\nabla \vec{u})^T)] + \rho \vec{g} + \vec{F}_{csf} \tag{4}$$

Energy equation:

$$\frac{\partial}{\partial t}(\rho E) + \nabla.[\vec{u}(\rho E + P)] = \nabla.(\lambda_{eff} \nabla T) + S_e \tag{5}$$

The surface tension force acting in the fluid throughout the interface is accounted for using the model proposed by Brackbill et al. (1992), called the continuous surface force (CSF) model, which treats this force as a pressure jump through the liquid-vapor interface as follows:

$$\vec{F}_{csf} = 2\sigma \frac{\alpha_l \rho_l \zeta_v \nabla \alpha_v + \alpha_v \rho_v \zeta_l \nabla \alpha_l}{\rho_l + \rho_v} \tag{6}$$

where ξ is the local interface curvature of each phase calculated as the volume fraction scalar gradient according to the formula below:

$$\zeta_l = \frac{\Delta \alpha_l}{|\nabla \alpha_l|} \tag{7}$$

$$\zeta_v = \frac{\Delta \alpha_v}{|\nabla \alpha_v|} \tag{8}$$

2.2 Phase Change Modeling

For an accurate simulation of the subcooled flow boiling process, the mass and heat transfer rates must be correctly estimated with an appropriate model. Therefore, in this study, the prediction of mass transfer rate is accomplished by the robust Lee model (Lee 1980), which depends on the saturation temperature (T_{sat}). It should be noted that at the liquid-vapor interface, the saturation temperature (T_{sat}) is constant. Subsequently, this model provides the mass transfer rates (S_l and S_v) with the following expressions:

If $T_l > T_{sat}$: evaporation occurs, therefore:

$$S_l = \alpha_l \rho_l \frac{(T_l - T_{sat})}{T_{sat}} \tag{9}$$

If $T_v < T_{sat}$: condensation occurs, therefore:

$$S_v = \alpha_v \rho_v \frac{(T_v - T_{sat})}{T_{sat}} \tag{10}$$

Then, the energy source term (S_e) can be found as a function of the mass transfer rate as follows:

$$S_e = -h_{lv} S_l = h_{lv} S_v \qquad (11)$$

2.3 Computational Domain and Boundary Conditions

This paper simulates the subcooled flow boiling behavior along two different minichannel configurations (straight and periodic constriction expansion). The details of the various designs and dimensions are depicted in Fig. 1. A shape ratio (k) is defined as equal to 1 for the straight shape and 0.6 for the periodic constriction expansion design.

The minichannel is in vertical upflow orientation toward the y-axis. In either configuration, the total length of the minichannel is equal to 144.6 mm, where 114.6 mm is heated, and 30 mm is adiabatic to remove the disturbances at the outlet. The working fluid is FC-72, and the solid material is copper. Besides, it is necessary to note that the dimensions of the straight minichannel are identical to the experimental study of Lee et al. (2019) to validate the present numerical model with their experimental results.

A constant mass flux boundary condition is applied to the inlet of the minichannel, and the inlet temperature is subcooled. Furthermore, we have imposed the pressure boundary condition on the minichannel outlet. The value of 380 K is set to the backflow temperature, which could be used if any reverse flow is generated, but it does not affect the numerical solution if no reverse flows are generated. Moreover, a uniform heat flux is specified for the heated walls, while the unheated walls are fixed to have adiabatic boundary conditions. All the inner walls are considered no-slip boundary conditions. The adhesion effects between the fluid and the walls are activated in the VOF mixture at 0.008 N/m, and the saturation temperature is 335.35 K. The initial state of the process is treated as stationary. In addition, the fluid and solid domains are initialized with the inlet boundary temperature.

2.4 Numerical Simulation Procedure

The different numerical procedures used to discretize the governing equations are presented in Table 1. Furthermore, a time step (Δt) that varies in the range of 10^{-4} to 10^{-6} is employed to keep the Courant number (Co) less than 0.5, thus making the numerical calculation stable and robust. Additionally, the computational model converges once the residuals of mass and velocity are less than 10^{-4} and the temperature residual is below 10^{-6}.
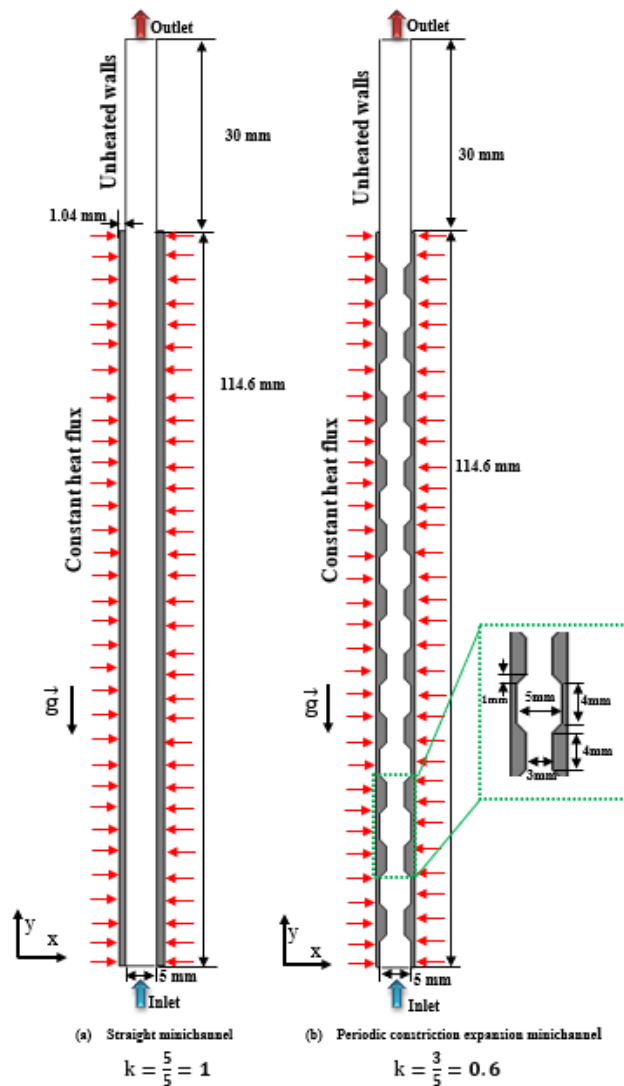

Fig. 1 Schematics diagram of computational domain (a) straight and (b) periodic constriction-expansion minichannel

Table 1 Numerical methods

Equation	Numerical method
Pressure-velocity coupling	PISO algorithm
Gradient	The green-gauss node-based method
Pressure	PRESTO
Momentum	Second order upwind scheme
Volume fraction	Geo-Reconstruct
Turbulent kinetic energy	First-order implicit scheme
Specific dissipation rate	First-order implicit scheme
Energy	Second order upwind scheme
Transient formulation	First-order implicit scheme

2.5 Grid Independence Study

The great quality of the mesh (orthogonal quality, skewness, and aspect ratio) significantly impacts the numerical simulation efficiency. Therefore, performing a grid independence test is crucial to achieving a mesh with a reasonable quality that allows for equilibrating the numerical cost and the accuracy of the solution. In this work, for both minichannel configurations, the mesh independence test is achieved for the mass flux of 836.64 kg/m²s under a uniform heat input of 191553 W/m² and subcooled temperature setting of 304.54 K.

The computational domains of the straight and the periodic constriction-expansion minichannel are meshed using a quadrilateral mesh, as shown in Fig. 2. Moreover, to capture the smaller bubbles generated near the walls, we have made treatments in the regions of the near wall as described in Fig. 2 based on y^+, which has a very important impact on flow and heat transfer characteristics. y^+ is specified as:

$$y^+ = \frac{\rho y \mu_\tau}{\mu} \qquad (12)$$

where y is the thickness of the first layer from the wall and is the friction velocity. Therefore, to treat the viscose sublayer region we have tried different values of y (1e⁻⁵; 8e⁻⁶; 7e⁻⁶ and 6e⁻⁶) which validates the condition that y^+ must be less than 5. Furthermore, five different cell sizes (3e⁻⁴; 2e⁻⁴; 1e⁻⁴; 8e⁻⁵; and 6e⁻⁵) are tested, corresponding respectively to 33540; 46696; 140970; 205495 and 343760 total number of grids.
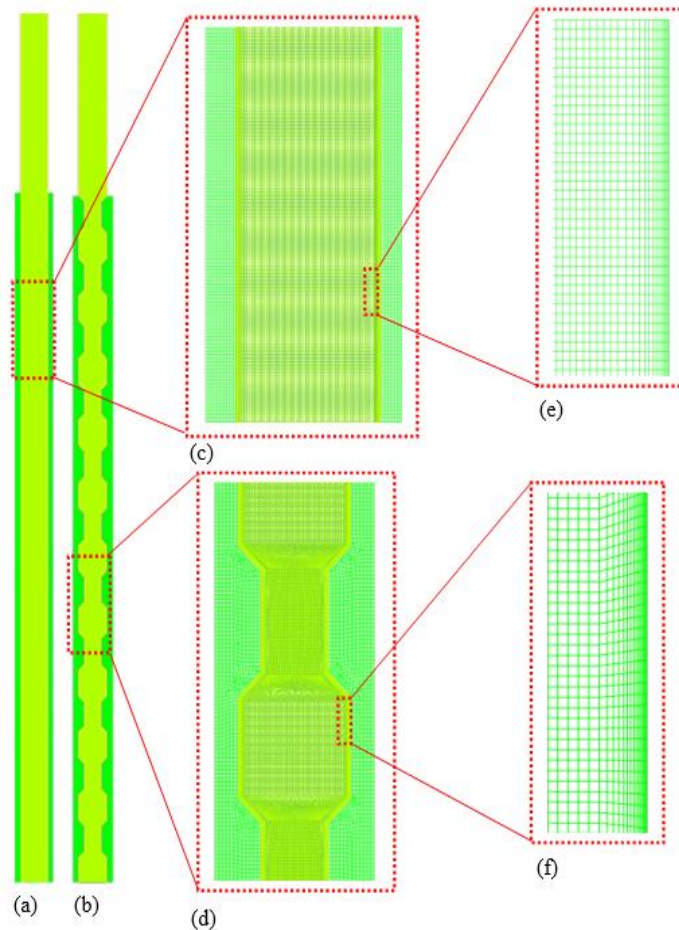

Fig. 2 Computational grids for the simulation domain of the (a) straight and (b) periodic constriction-expansion minichannel; (c) zoomed-in view of the straight design; (d) zoomed-in view of the periodic constriction-expansion design; (e) enlarged view close to the boundary wall of the straight minichannel and (f) enlarged view close to the boundary of the periodic constriction-expansion minichannel
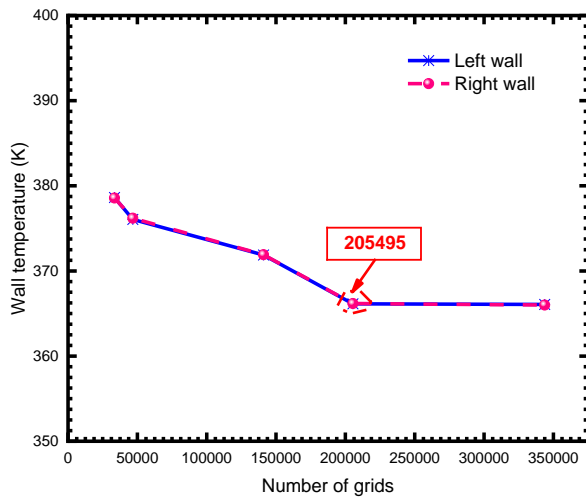
Fig. 3 Grid independence test results

Fig. 4 Heat transfer coefficient comparison between experimental data and present simulation results

Figure 3 presents the mesh independence test results in terms of the area-weighted average wall temperature according to the total amount of grids. It appears that an increase in the number of grids (cell size decreases) reduces the average wall temperature until the grid with 205495 nodes (cell size = $8e^{-5}$), in which the temperature becomes unchanged according to the grid number, i.e., independent of the mesh size.

A finer mesh provides a better resolution. Nevertheless, due to the requirement to balance the accuracy of the solution with the computation time, we have selected for all cases the grid with the cell size of 8e-4 and the value of 6e-6 for y.

2.6 Validation

To confirm the accuracy of the current numerical model, the straight minichannel with boundary conditions of constant mass flux (836.64 kg/m²s), inlet temperature (304.54 K), and heat flux (191552 W/m²) is simulated and compared to the results of Lee et al. (2019), found along the identical dimensions of the straight minichannel and under the same working conditions (working fluid, mass flux, heat flux, and inlet temperature).

Figure 4 compares the computed local heat transfer coefficients in the left and right walls to the experimental results reported by Lee et al. (2019). From this figure, the mean errors of 6.39% and 9.78%, were recorded between the currently calculated finding and the experimental data. It is important to take into account that the uncertainty, as well as errors, met in the experiments are the main reasons for this small divergence from the experimental results.

Furthermore, Fig. 5 illustrates a further comparison flow regimes visualization of the experimentation of Lee et al. (2019) with the currently CFD simulations results. As is clearly shown, flow patterns behavior and evolution are predicted with a remarkable degree of precision, which demonstrates that the present numerical simulation is very accurate and efficient.
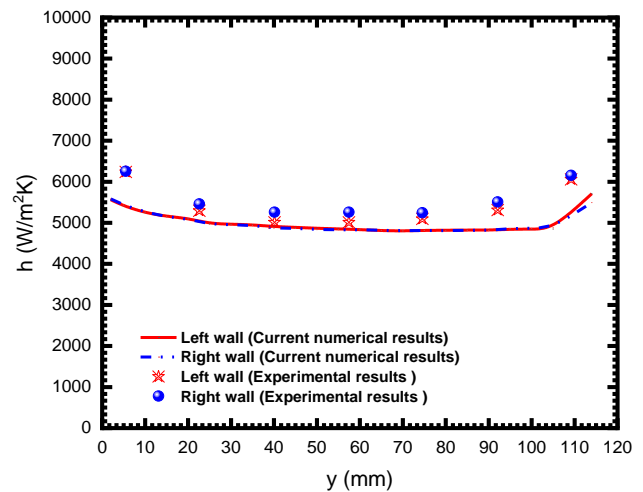
3. RESULTS AND DISCUSSIONS

The flow patterns behavior, as well as the thermal transfer characteristics and pressure drop of the subcooled flow boiling in response to the influence of minichannel shape, are evaluated using CFD simulations by ANSYS Fluent software. In addition, to find out whether the mass flux will be a critical factor in the flow pattern characteristics of subcooled flow boiling, simulations of both configurations (straight and periodic constriction-expansion) are performed for four mass fluxes, that are G= 500 kg/m²s; 836.64 kg/m²s; 1170 kg/m²s; and 2535 kg/m²s (i.e., *Re* = 6500.26; 10876.75; 15210.60; and 32956.31) at a constant heat flux and an inlet temperature. In subcooled flow boiling, nucleation begins as the fluid reaches its saturation temperature, which is then followed by bubble coalescence. Fig.6 presents the results of the two-phase flow pattern along the two minichannel configurations. This figure shows that, for all designs, a very poor rate of bubble nucleation is stimulated in the inlet region due to the subcooling temperature, which leads to high retardation on reaching the saturation temperature. Besides, the position where nucleation occurred moved further away from the inlet as the mass flux increased. Thereafter, the generation of bubbles begins to increase owing to the active subcooled boiling. In the case of a straight minichannel, Fig. 6 shows that at a low mass flux of 500 kg/m²s, the fluid region is occupied by large vapor bubbles due to high bubble coalescence, and the bubble size decreases as the mass flux increases, which leads to a dominant bubbly flow with relatively small bubbles. This is mostly because, at a low mass flux, the heat absorbed by the liquid phase from the heated walls is much more important, and therefore a considerable amount of liquid is changed to vapor. However, at high mass flux, the fluid moves with a higher velocity, limiting the fluid-wall interactions, which induce significant retardation in phase change. In the case of the periodic constriction expansion minichannel, Fig. 6 shows the presence of dispersed bubbly flow for almost all mass fluxes with a decrease in bubble size as the mass flux
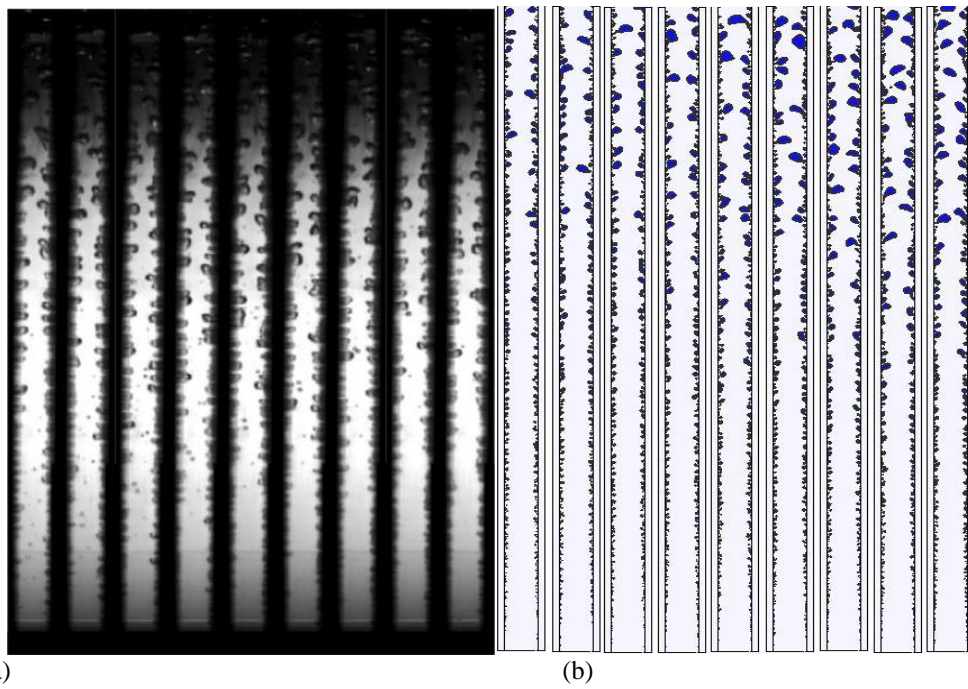
Fig. 5 Comparison of the (a) experimental data of Lee et al. (2019) and (b) simulation results in terms of flow patterns
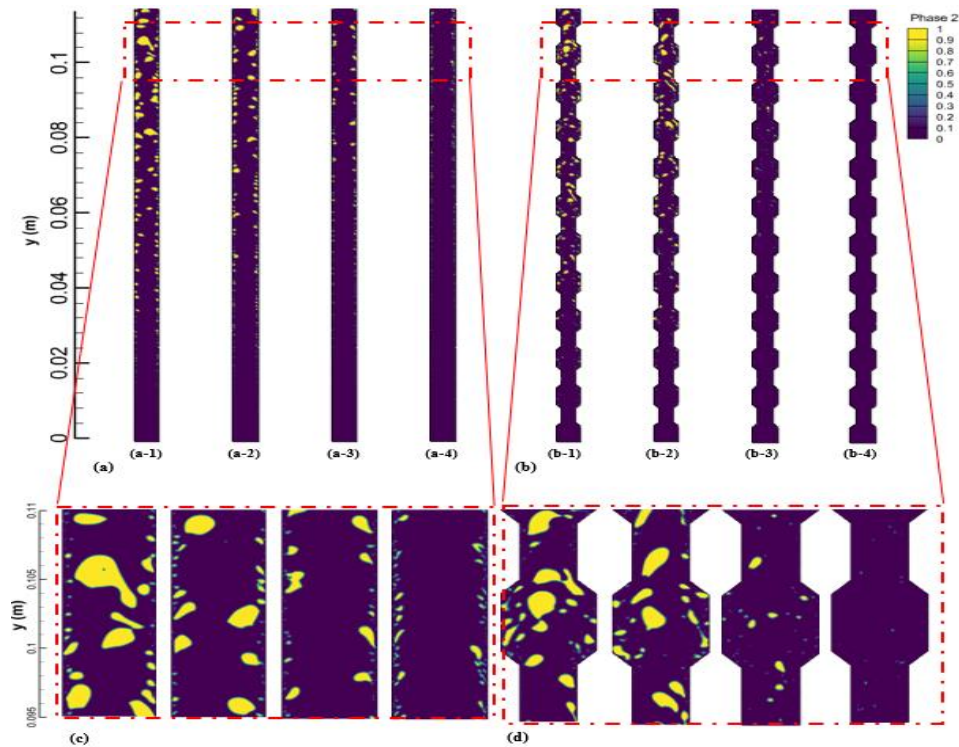

Fig. 6 Flow patterns as a function of mass fluxes in the (a) straight and (b) periodic constriction-expansion minichannels; (a-1) and (b-1) G =500 kg/m^2 s; (a-2) and (b-2) G =836.64 kg/m^2 s; (a-3) and (b-3) G =1170 kg/m^2 s; (a-4) and (b-4) G =2535 kg/m^2 s

increases, which is related to the improved inertia and buoyancy forces in the constriction expansion cross-sections. Furthermore, in the periodic constriction-expansion minichannel, the thermal boundary layers are periodically disrupted and redeveloped as a result of the abrupt expansion of the cross-sections, leading to a small total thickness of the thermal boundary layers, which leads

to a good mixing between layers that contribute to the significant detachment of bubbles from the walls. As a result, as the minichannel changes from a straight to a periodic constriction-expansion design, the initiation of

bubble nucleation changes, resulting in a different bubbly flow pattern and a variety of heat transfer characteristics. The axial evolution of the heat transfer
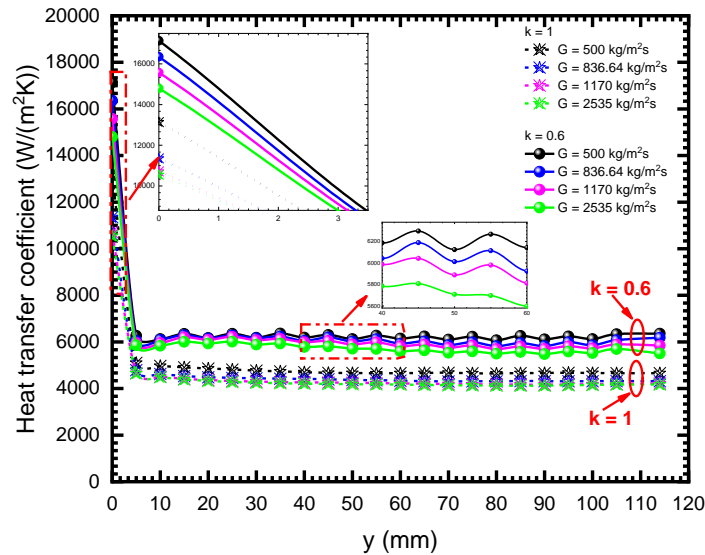
Fig. 7 Variation of local heat transfer coefficient along the periodic constriction-expansion minichannel (k = 0.6) and the straight minichannel (k = 1) for different mass fluxes

coefficients through the straight (k = 1) and periodic constriction-expansion (k = 0.6) minichannels for different mass fluxes are presented in Fig. 7. This figure shows that in the inlet of the minichannel, the heat transfer coefficients are significantly greater than those in all other locations throughout the minichannel in both configurations and for all mass fluxes due to a rise in flow perturbation caused by an abrupt flow contraction. Because of the increased thermal boundary layer thickness effects, the thermal transfer coefficient decreases gradually along the straight shape. However, in the case of k = 0.6, the local heat transfer coefficient varies periodically due to the sinusoidal solid-fluid interface generated by the periodic constriction and expansion sections. The heat transfer coefficient reaches the highest values in the constriction sections and the lowest values in the expansion sections because the flow velocity varies evidently with the cross-section variation.

Figure 7 also displays that for all minichannel shapes, the heat transfer coefficient reduces with increasing mass flux due to the quasi-inactivation of a large proportion of nucleation sites caused by the growth of the flow velocity. Furthermore, it can be seen that for all mass fluxes, the heat transfer coefficients in the periodic constriction expansion minichannel (k = 0.6) are significantly higher than those of k = 1. The heat transfer is enhanced by 43.12% for G = 500 kg/m²s and 22.14% for G = 2535 kg/m²s. This remarkable enhancement can be attributed to the fact that the periodic constriction sections cause a significant expansion of the heat transfer area, resulting in more favorable fluid mixing between the near-wall flow and the core flow regions.

Figure 8 depicts the isotherm's contours for different mass fluxes. In all cases, the temperature is high close to the walls and low at the minichannel center. Furthermore, it is observed that the cold core flow volume diminishes in the case of k = 0.6 compared to that of k = 1, which is a sign of good flow mixing between the hot flow near the walls and the cold core flow, which demonstrates the

beneficial effects of the periodic expansion cross-sections. However, this cold core flow volume grows as the mass flux increases because the flow becomes highly disturbed with the increase in flow velocity, which interrupts interactions between layers.

The pressure drop is another critical parameter that acts on the subcooled flow boiling performances in the minichannel. Figure 9 displays the pressure drop average variation caused by the effect of mass flux along the two minichannel designs. It can be observed that in both configurations, as the mass flow increases, the pressure drop also becomes more pronounced due to the growth of the flow velocity. Compared to the straight design, the periodic constriction expansion exhibits a 4.32–8.36% increase in pressure drop for a mass flux of 500–2535 kg/m²s. This is because the pressure drop in the periodic constriction expansion design is the combined pressure drop along the minichannel that resulted from the periodic constriction and expansion regions. Furthermore, these cross-sections are responsible for creating the body drag force as well as the widening of the turbulence.

4. SUMMARY AND CONCLUSIONS

The thermal performance, pressure drop, and flow patterns behavior of subcooled flow boiling in different configurations of a vertical minichannel are explored through 2D numerical simulations. A new periodic constriction-expansion design is put forward, studied, and compared to the straight minichannel to determine the appropriate configuration that enhances heat transfer. The simulations are performed for several mass fluxes.

The major highlights that can be extracted from this work are outlined as follows:

1. The present CFD simulation results are in reasonable accord with the previous experimental findings, with mean relative errors of 6.39% and 9.78%.
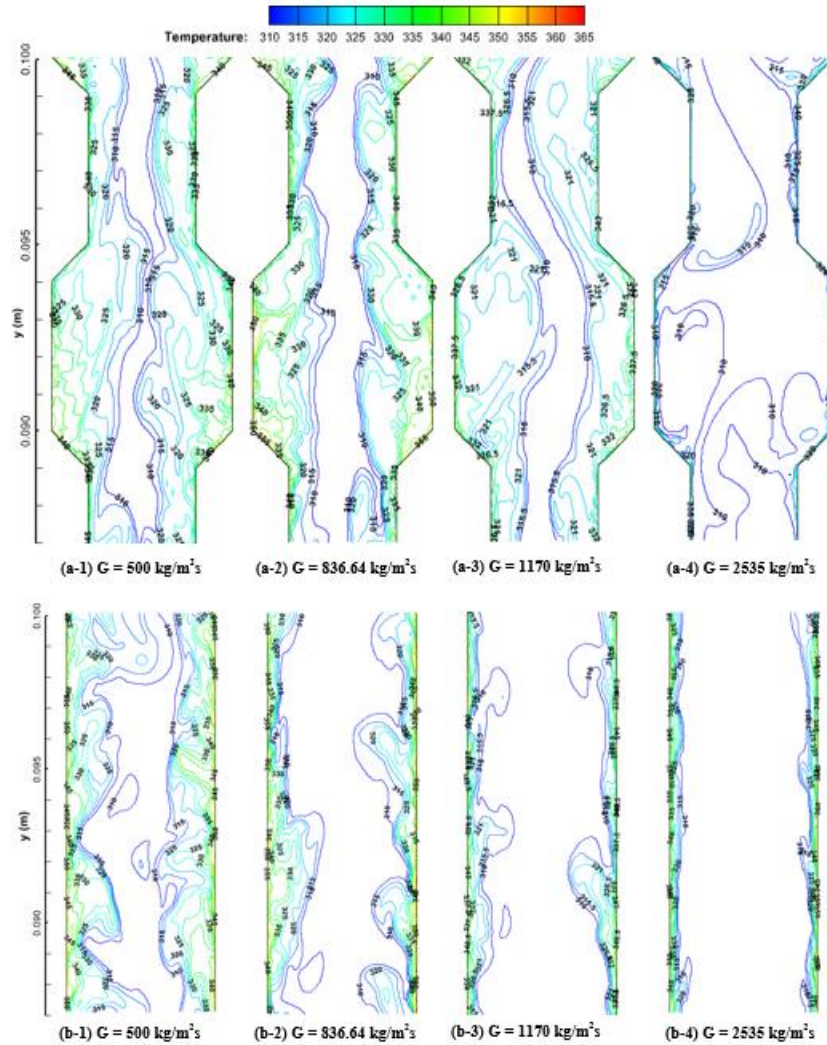
Fig. 8 Isotherms contours in the (a) periodic constriction-expansion and (b) straight minichannel as a function of mass flux
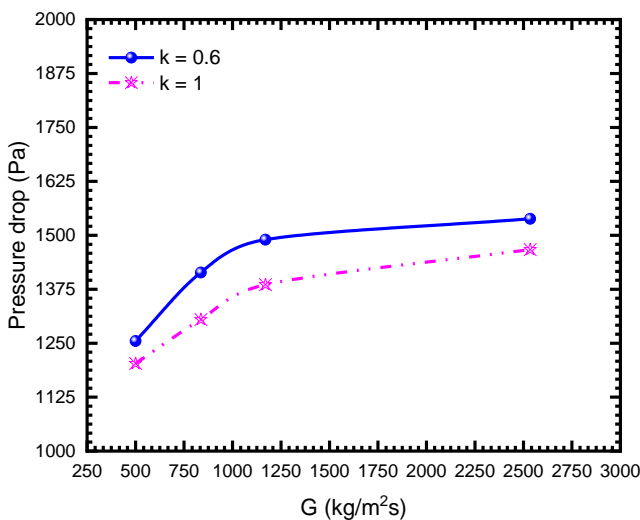

Fig. 9 Pressure drop in the periodic constriction-expansion minichannel (k = 0.6) and straight minichannel (k = 1) as a function of mass flux

2. In both configurations, the rise of the mass flux leads to a decrease in the heat transfer coefficient.

3. The heat transfer coefficient varies periodically along the periodic constriction-expansion minichannel due to the sinusoidal solid-fluid interface generated by the periodic constriction and expansion cross-sections. In addition, the amplitude of fluctuations decreases as the mass flux increases.

4. The periodic constriction expansion configuration exhibited good mixing between the hot flow near the walls and the cold core flow, as well as a meaningful effect on the temperature distribution. Furthermore, this design recorded the greatest enhancement in heat transfer (22.14–43.11% for G from 500 kg/m^2s to 2535 kg/m^2s).

The current numerical study demonstrates that using subcooled flow boiling in the periodic constriction-expansion configuration is an appropriate approach that results in the greatest improvement in thermal

performance. Therefore, extending the cooling device's life and eliminating any damage due to overheating.

AUTHOR CONTRIBUTIONS

A. Igaadi carried out and developed the numerical model, simulations, validation, data curation and prepared the original manuscript; H. El Mghari examined the manuscript; R. El Amraoui supervised the work.

CONFLICT OF INTEREST

The authors declared no potential conflicts of interest concerning the research, authorship, and publication of this article.

REFERENCES

Agostini, B., Fabbri, M., Park, J. E., Wojtan, L., Thome, J. R. & Michel, B. (2007). State of the art of high heat flux cooling technologies. *Heat Transfer Engineering*, 28(4), 258-281. https://doi.org/10.1080/01457630601117799

Ahmadi, R., Ueno, T., & Okawa, T. (2012). Bubble dynamics at boiling incipience in subcooled upward flow boiling. *International Journal of Heat and Mass Transfer*, 97, 114-125. https://doi.org/10.1016/j.ijheatmasstransfer.2011.09.050

Ahmadi, R., & Okawa, T. (2015). Influence of surface wettability on bubble behavior and void evolution in subcooled flow boiling. *International Journal of Thermal Sciences*, 97, 114-125. https://doi.org/10.1016/j.ijthermalsci.2015.06.012

Ali, R., & Palm, B. (2011). Dryout characteristics during flow boiling of R134a in vertical circular minichannels. *International Journal of Heat and Mass Transfer*, 54, 2434-2445. https://doi.org/10.1016/j.ijheatmasstransfer.2011.02.018

Azzolin, M., & Bortolin, S. (2021). Condensation and flow boiling heat transfer of a HFO/HFC binary mixture inside a minichannel. *International Journal of Thermal Sciences,* 159, 106638. https://doi.org/10.1016/j.ijthermalsci.2020.106638

Bahreini, M., Ramiar, A., & Ranjbar, A. A. (2015). Numerical simulation of bubble behavior in subcooled flow boiling under velocity and temperature gradient. *Nuclear Engineering and Design*, 238-248. https://doi.org/10.1016/j.nucengdes.2015.08.004

Bahreini, M., Ramiar, A., & Ranjbar, A. A. (2016). Numerical Simulation of Subcooled Flow Boiling under Conjugate Heat Transfer and Microgravity Condition in a Vertical Mini Channel. *Applied Thermal Engineering*, 170-185. https://doi.org/10.1016/j.applthermaleng.2016.11.016

Boure, J. A., Bergles, A. E., & Tong, L. S. (1973). Review of two-phase flow instability. *Nuclear Engineering and Design*, 25(2), 165-192. https://doi.org/10.1016/0029-5493(73)90043-5

Bower, J. S., & Klausner, J. F. (2006). Gravity independent subcooled flow boiling heat transfer regime. *Experimental Thermal and Fluid Science.* 10.1615/ICHMT.2004.IntThermSciSemin.720

Brackbill, J. U., Kothe, D. B., & Zemach, C. (1992). A continuum method for modeling surface tension. *Journal of Computational Physics*, 100, 130-139. https://doi.org/10.1016/0021-9991(92)90240-Y

Brutin, D., Ajaev, V. S., & Tadrist, L. (2013). Pressure drop and void fraction during flow boiling in rectangular minichannels in weightlessness. *Applied Thermal Engineering*, 51, 1317-1327. https://doi.org/10.1016/j.applthermaleng.2012.11.017

Chai, L., Xia, G., Wang, L., Zhou, M., & Cui, Z. (2013), Heat transfer enhancement in microchannel heat sinks with periodic expansion–constriction cross-sections. *International Journal of Heat and Mass Transfer*, 62, 741-751. https://doi.org/10.1016/j.ijheatmasstransfer.2013.03.045

Chang, W., Zhang, S. S., Tian, S., & Huo, M. J. (2011). Research on the flow boiling and heat transfer of ethanol in a corrugated mini-channel. *Applied Mechanics and Materials*, 66–68. https://doi.org/10.4028/www.scientific.net/AMM.66-68.876.

Chen, A., Lin, T. F., Ali, H. M., & Yan, W. M. (2020). Experimental study on bubble characteristics of time periodic subcooled flow boiling in annular ducts due to wall heat flux oscillation. *International Journal of Heat and Mass Transfer*, 157, 119974. https://doi.org/10.1016/j.ijheatmasstransfer.2020.119974

Chen, C. A., Li, K. W., Lin, T. F., Li, W. K., & Yan, W. M. (2021). Study on heat transfer and bubble behavior inside horizontal annuli: Experimental comparison of R-134a, R–407C, and R-410A subcooled flow boiling. *Case Studies in Thermal Engineering,* 24, 100875. https://doi.org/10.1016/j.csite.2021.100875

Gao, W., Xu, X., & Liang, X. (2017). Experimental study on the effect of orientation on flow boiling using R134a in a mini-channel evaporator. *Applied Thermal Engineering*, 121, 963-973. https://doi.org/10.1016/j.applthermaleng.2017.04.019

Hirt, C. W., Nichols, B. D. (1981). Volume of fluid (VOF) method for the dynamics of free boundaries, *Journal of Computational Physics*,39(1), 201-225. https://doi.org/10.1016/0021-9991(81)90145-5

Hożejowska, S., Kaniowski, R. M., & Poniewski, M. E. (2016). Experimental investigations and numerical modeling of 2D temperature fields in flow boiling in minichannels. *Experimental Thermal and Fluid Science*, 78, 18-29. https://doi.org/10.1016/j.expthermflusci.2016.05.005

Hsu, W. T., Lee, N., Lee, D., Kim, J., Yun, M., & Cho, H. H. (2022). Surfaces with bent micro-polymerized pillars exhibit enhanced heat transfer during subcooled flow boiling. *International Journal of Heat and Mass Transfer*, 182, 121941. https://doi.org/10.1016/j.ijheatmasstransfer.2021.121941

Huang, P., & Pan, M. (2021). Secondary heat transfer enhancement design of variable cross-section microchannels based on entrancy analysis. *Renewable and Sustainable Energy Reviews*, 141, 110834. https://doi.org/10.1016/j.rser.2021.110834

Huang, P. G. D., Zhong, X., & Pan, M. (2020). Numerical investigation of the fluid flow and heat transfer characteristics of tree-shaped microchannel heat sink with variable cross-section. *Chemical Engineering and Processing - Process Intensification*, 147, 107769. https://doi.org/10.1016/j.cep.2019.107769

Iceri, D. M., Zummo, G., Saraceno, L., & Ribatski, G. (2020). Convective boiling heat transfer under microgravity and hypergravity conditions. *International Journal of Heat and Mass Transfer*, 119614. https://doi.org/10.1016/j.ijheatmasstransfer.2020.119614

Igaadi, A., El Mghari, H., & El Amraoui, R. (2023). Numerical investigation into the effects of orientation on .Subcooled Flow Boiling Characteristics*Journal of Applied and Computational Mechanics*. https://doi.org/10.22055/JACM.2022.41723.3802

Kandlikar, S. G. (2012). History, advances, and challenges in liquid flow and flow boiling heat transfer in microchannels: A critical review. *ASME Journal of Heat and Mass Transfer*, 134(3), 034001. https://doi.org/10.1115/1.4005126

Kennedy, J. E., Roach Jr, G. M., Dowling, M. F., Abdel-Khalik, S. I., Ghiaasiaan, S. M., Jeter, S. M., & Quershi, Z. H. (2000), The onset of flow instability in uniformly heated horizontal microchannels. *Journal of Heat and Mass Transfer*, 122(1), 118-125. https://doi.org/10.1115/1.521442

Kim, S. J., McKrell, T., Buongiorno, J., & Hu, L. (2010). Subcooled flow boiling heat transfer of dilute alumina, zinc oxide, and diamond nanofluids at atmospheric pressure. *Nuclear Engineering and Design*, 240, 1186-1194. https://doi.org/10.1016/j.nucengdes.2010.01.020

Lebon, M. T., Hammer, C. F., & Kim, J. (2019). Gravity effects on subcooled flow boiling heat transfer. *International Journal of Heat and Mass Transfer*, 128, 700-714. https://doi.org/10.1016/j.ijheatmasstransfer.2018.09.011

Lee, J., O'Neill, L. E., Lee, S., & Mudawar, I. (2019). Experimental and computational investigation on two-phase flow and heat transfer of highly subcooled flow boiling in vertical upflow. *International Journal of Heat and Mass Transfer*, 136, 1199-1216. https://doi.org/10.1016/j.ijheatmasstransfer.2019.03.046

Lee, S. W., Kim, K. M., & Bang, I. C. (2013). Study on flow boiling critical heat flux enhancement of graphene oxide/water nanofluid. *International Journal of Heat and Mass Transfer*, 65, 348-356. https://doi.org/10.1016/j.ijheatmasstransfer.2013.06.013

Lee, W. H. (1980). Pressure iteration scheme for two-phase flow modeling. *Multiphase Transport: Fundamentals, Reactor Safety, Applications*, 407-432.

Li, Y., Xia, G., Jia, Y., Cheng, Y., & Wang, J. (2017). Experimental investigation of flow boiling performance in microchannels with and without triangular cavities–A comparative study. *International Journal of Heat and Mass Transfer*, 108, 1511-1526.

Li, Y. F., Xia, G. D., Ma, D. D., Yang, J. L., & Li, W. (2020). Experimental investigation of flow boiling characteristics in microchannel with triangular cavities and rectangular fins. *International Journal of Heat and Mass Transfer*, 148, 119036.

Liu, Z., Bi, Q., Guo, Y., & Su, Q. (2012). Heat transfer characteristics during subcooled flow boiling of a kerosene kind hydrocarbon fuel in a 1mm diameter channel. *International Journal of Heat and Mass Transfer*, 55, 4987-4995. https://doi.org/10.1016/j.ijheatmasstransfer.2012.04.039

Liu, Z., & Bi, Q. (2015). Onset and departure of flow boiling heat transfer characteristics of cyclohexane in a horizontal minichannel. *International Journal of Heat and Mass Transfer*, 88, 398-405. https://doi.org/10.1016/j.ijheatmasstransfer.2015.04.088

Manda, U., Peles, Y., & Putnam, S. (2021). *Comparison of heat transfer characteristics of flow of supercritical carbon dioxide and water inside a square microchannel.* 20th IEEE Intersociety Conference on Thermal and Thermomechanical Phenomena in Electronic Systems (iTherm), 1207-1213. https://doi.org/10.1109/ITherm51669.2021.9503192

Manda, U., Parahovnik, A., & Peles, Y. (2022). Thermoacoustic waves and piston effect inside a microchannel with carbon dioxide near critical conditions. *Thermal Science and Engineering Progress*, 36, 101528. https://doi.org/10.1016/j.tsep.2022.101528

Manda, U., Parahovnik, A., & Peles, Y. (2020). *Theoretical investigation of boundary layer behavior and heat transfer of supercritical carbon dioxide (Sco2) in a microchannel.* Itherm-2020 conference, Orlando, FL, USA, 888-892. https://doi.org/10.1109/ITherm45881.2020.9190408

Markal, B., Candan, A., Aydin, O., & Avci, M. (2018a). Experimental investigation of flow boiling in single minichannels with low mass velocities. *International Communications in Heat and Mass Transfer*, 98, 22-30.

https://doi.org/10.1016/j.icheatmasstransfer.2018.08.002

Markal, B., Candan, A., Aydin, O., & Avci, M. (2018b). Critical heat flux at flow boiling of refrigerants in minichannels at high reduced pressure. *International Journal of Heat and Mass Transfer*, 122, 732-739. https://doi.org/10.1016/j.ijheatmasstransfer.2018.02.027

McGlen, R. J., Jachuck, R., & Lin, S. (2004). Integrated thermal management techniques for high power electronic devices. *Applied Thermal Engineering*, 24 (8–9), 1143-1156. https://doi.org/10.1016/j.applthermaleng.2003.12.029

Nedaei, M., Motezakker, A. R., Zeybek, M. C., Sezen, M., Ozaydin, I. G., & Kosar, A. (2017). Subcooled flow boiling heat transfer enhancement using polyperfluorodecylacrylate (pPFDA) coated microtubes with different coating thicknesses. *Experimental Thermal and Fluid Science*, 86, 130-140. https://doi.org/10.1016/j.expthermflusci.2017.04.008

Parahovnik, A., & Peles, Y. (2022). Bubble dynamics in a subcooled flow boiling of near-critical carbon dioxide. *International Journal of Heat and Mass Transfer*, 183, 122191. https://doi.org/10.1016/j.ijheatmasstransfer.2021.122191

Parahovnik, A., Manda, U., & Peles, Y. (2022). Heat transfer mode shift to adiabatic thermalization in near-critical carbon dioxide with flow boiling in a microchannel. *International Journal of Heat and Mass Transfer*, 188, 122629. https://doi.org/10.1016/j.ijheatmasstransfer.2022.122629

Phan, H. T., Caney, N., Marty, P., Colasson, S., & Gavillet, J. (2011). Flow boiling of water in a minichannel: The effects of surface wettability on two-phase pressure drop. *Applied Thermal Engineering*, 31, 1894-1905. https://doi.org/10.1016/j.applthermaleng.2011.02.036

Piasecka, M., & Strąk, K. (2019). Influence of the surface enhancement on the flow boiling heat transfer in a minichannel. *Heat Transfer Engineering*, 40(13-14), 1162-1175. https://doi.org/10.1080/01457632.2018.1457264

Piasecka, M. (2012). An application of enhanced heating surface with mini-reentrant cavities for flow boiling research in minichannels. *Heat Mass Transfer*. https://doi.org/10.1007/s00231-012-1082-y

Piasecka, M. (2013). Heat transfer mechanism, pressure drop and flow patterns during FC-72 flow boiling in horizontal and vertical minichannels with enhanced walls. *International Journal of Heat and Mass Transfer*, 66, 472-488. https://doi.org/10.1016/j.ijheatmasstransfer.2013.07.046

Piasecka, M. (2014). The use of enhanced surface in flow

boiling heat transfer in a rectangular minichannel. *Experimental Heat Transfer: A Journal of Thermal Energy Generation, Transport, Storage, and Conversion,* 231-255. https://doi.org/10.1080/08916152.2013.782374

Prajapati, Y. K., Pathak, M., & Khan, M. K. (2015). A comparative study of flow boiling heat transfer in three different configurations of microchannels. *International Journal of Heat and Mass Transfer*, 711-722. https://doi.org/10.1016/j.ijheatmasstransfer.2015.02.016

Ramasamy, N. S., Kumar, P., Wangaskar, B., Khandekar, S., & Maydanik, Y. F. (2018), Miniature ammonia loop heat pipe for terrestrial applications: Experiments and modeling. *International Journal of Thermal Sciences*, 124, 263-278. https://doi.org/10.1016/j.ijthermalsci.2017.10.018

Rena, T., Zhub, Z., Shi, J., Yana, C., & Zhanga, R. (2020). Experimental study on bubble sliding for upward subcooled flow boiling in a narrow rectangular channel. *International Journal of Heat and Mass Transfer*, 119489. https://doi.org/10.1016/j.ijheatmasstransfer.2020.119489

Şişman, Y., Khalili Sadaghiani, A., Khedir, R., Brozak, M., Karabacak, T., & Koşar, A. (2016). Subcooled flow boiling over microstructured plates in rectangular minichannels. *Nanoscale and Microscale Thermophysical Engineering*, 20(3-4), 173-190. https://doi.org/10.1080/15567265.2016.1248584

Sugrue, R., Buongiorno, J., & McKrell, T. (2014). An experimental study of bubble departure diameter in subcooled flow boiling including the effects of orientation angle, subcooling, mass flux, heat flux, and pressure. *Nuclear Engineering and Design*, 182-188. https://doi.org/10.1016/j.nucengdes.2014.08.009

Sun, Y., Zhang, L., Xu, H., & Zhong, X. (2011). Subcooled flow boiling heat transfer from microporous surfaces in a small channel. *International Journal of Thermal Sciences,* 881-889. https://doi.org/10.1016/j.ijthermalsci.2011.01.019

Tardist, L. (2007). Review on Two-Phase Instabilities in Narrow Spaces. *International Journal of Heat and Fluid Flow*, 28(1), 54–62. https://doi.org/10.1016/j.ijheatfluidflow.2006.06.004

Tiwari, N., & Moharana, M. K. (2021). Conjugate effect on flow boiling instability in wavy microchannel. *International Journal of Heat and Mass Transfer*, 120791. https://doi.org/10.1016/j.ijheatmasstransfer.2020.120791

Vasileiadou, P., Sefiane, K., Karayiannis, T. G., & Christy, J. R. E. (2017). Flow boiling of ethanol/water binary mixture in a square mini-channel. *Applied Thermal Engineering*, 127, 1617-1626. https://doi.org/10.1016/j.applthermaleng.2017.08.126

Wang, Y., & Wu, J. M. (2015). Numerical simulation on single bubble behavior during Al2O3/H2O nanofluids flow boiling using Moving Particle Simi-implicit method. *Progress in Nuclear Energy*, 85, 130-139. https://doi.org/10.1016/j.pnucene.2015.06.017

Zhou, G., Li, J., & Lv, L. (2016). An ultra-thin miniature loop heat pipe cooler for mobile electronics. *Applied Thermal Engineering*, 109 (Part A), 514-523. https://doi.org/10.1016/j.applthermaleng.2016.08.13 8

.